Excitable Spatio-Temporal Chaos in a Model of Glycolysis

Gerold Baier,*,† Markus Müller,‡ and Henrik Ørsnes‡

Facultad de Ciencias, Universidad Autónoma del Estado de Morelos, 62210 Cuernavaca, Morelos, México, and Physical Biochemistry Group, Institute of Biochemistry, South Danish University, DK-5230 Odense M, Denmark

Received: October 16, 2001; In Final Form: December 12, 2001

We study the spatio-temporal dynamics of a qualitative model of the glycolytic reaction catalyzed by phosphofructokinase. Adding the nonlinear regulation by fructose-2,6-bisphosphate, the model is found to exhibit complex oscillations and two types of chaos. In particular, a region of excitable chaos is found in parameter space. In a spatially extended system, this excitable chaos gives rise to spontaneous irregular spiking as well as self-organized formation of spots of high ATP concentration with "center-surround" characteristics. The deterministic spiking has noise-like temporal properties but shows a pronounced "memory", which we attribute to the transient aparition of a Turing-pattern that exists nearby in parameter space. The model thus provides an example of an excitable medium that prohibits (rather than permits) the propagation of concentration waves. This could be exploited by the living cell to self-organize pronounced local amplification of ATP.

Introduction

Can the nonlinear dynamics of glycolysis play a functional role in cellular information processing? Glycolysis—the biochemical pathway of glucose degradation—is known to play an important role in energy metabolism. The process results in the net synthesis of two molecules of adenosine triphosphate (ATP) per consumed molecule of glucose. However, it is also known that processes in the mitochondria utilizing acetyl CoA account for the majority (about 95%) of a typical cell's ATP production. Thus, one might question whether synthesis of ATP is the only metabolic role of this exquisitely elaborated pathway. Among other peculiarities, glycolysis has long been famous for its complex and strongly nonlinear net of feedback control mechanisms. These nonlinear control loops were assumed to be responsible for the experimentally observed nonlinear dynamics of glycolytic intermediates in cell free extracts from yeast.[1] Instances of concentration oscillations in mammalian cells include beef heart extracts,[2] sceletal muscle extracts,[3] and rat liver extracts.[4] It was immediately realized that phosphofructokinase (PFK-1), the key control enzyme in glycolysis, must play a major role in the mechanism of the oscillations. However, the metabolic function of these oscillations remained questionable.

The theoretical and experimental study of spatially extended biochemical reaction systems has demonstrated that nonlinear kinetics is an elegant means to generate complex self-organized spatio-temporal patterns. Rössler embedded the linear Turing model for spontaneous gradient formation in a set of nonlinear equations with enzyme kinetics and found two qualitatively different types of spatio-temporal chaos.[5] Several theoretical studies based on this early result concluded that chaotic (and hyperchaotic) spatio-temporal patterns (like phase turbulence, defect turbulence, labyrinthine chaos, and Hopf-Turing mixed modes) are a natural consequence of biochemical feedback regulation, be it positive[6,7] or negative.[8] Experimentally, non-chaotic pattern formation based on nonlinear kinetic feedback mechanisms was reported in frog eggs[9] and in unstirred cell-free extracts from yeast.[10,11] The analysis of recordings of complex concentration patterns of cytosolic calcium in rat hepatocytes following stimulation by ATP[12] has led to the hypothesis that deterministic chaotic spiking could be exploited as a means of intracellular information processing.[13] The observation of unambiguously chaotic oscillations during glycolysis in a continuous-supply stirred reactor[14,15] provides evidence that the glycolytic reaction network is capable of generating more than mere periodic patterns.

The crucial role of fructose-2,6-bisphosphate (Fru-2,6-P_2) in the control of the glycolytic pathway[16] was not known at the time when the bulk of the literature on glycolytic oscillations appeared, and it was not taken into account in mathematical models simulating glycolytic oscillations which appeared after this discovery.[17,18,19] Whereas Fru-2,6-P_2 does not seem to be necessarily required to generate simple periodic oscillations in yeast[20] or skeletal muscle extracts,[21] it was revealed by experimental studies that low concentrations of Fru-2,6-P_2 induce glycolytic oscillations and high concentrations of the effector abolish the oscillations.[22] Furthermore, it was found that Fru-2,6-P_2 is capable of inducing transitions between alternative glycolytic steady states in cell free extracts of rat liver.[23] In this paper, we present a model of a specifically mammalian glycolytic system with explicit participation of Fru-2,6-P_2. The model is based on known kinetic properties of rat liver enzymes.[24] Our investigations focus on excitable and self-exciting patterns due to the regulation by Fru-2,6-P_2, suggesting (for example) ATP as a candidate for a dynamic intracellular messenger.

Model

The aim of the model is to account for the nonlinear dynamics of the glycolytic pathway. In accordance with previous attempts, we focus on the behavior of the key regulatory enzyme PFK-1 and write down the expressions for a reaction in a continuous flow stirred tank reactor (CSTR). The reaction volume is taken

* Corresponding author. E-mail: baier@servm.fc.uaem.mx.
† Universidad Autónoma del Estado de Morelos.
‡ South Danish University.

10.1021/jp0138173 CCC: $22.00
Published on Web 03/05/2002

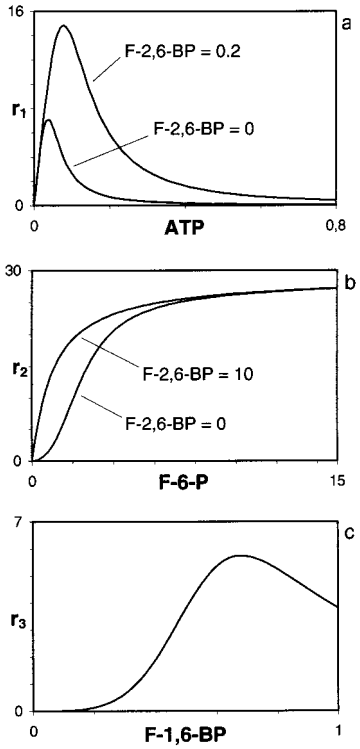

Figure 1. Dependencies of the individual rates r_i of the PFK-1 reaction. (a) r_1 as a function of [ATP] without and with [Fru-2,6-P_2]; $c_1 = 29$, $c_2 = 0.1$, $d = 1$. (b) r_2 as a function of [Fru-6-P] without and with [Fru-2,6-P_2]; $c_5 = 1$, $c_6 = 19$, $L = 80$. (c) r_3 as a function of [Fru-1,6-P_2].

to be constant, and ATP, Fru-6-P, Fru-2,6-P_2, PFK-1, and PFK-2 are supplied from a reservoir of constant concentrations at a constant rate. In reality, substrates and enzymes must be in different stock solutions. This can be realized experimentally[14] and feedstock concentrations and flow rates can be used as bifurcation parameters.

The enzyme PFK-1 catalyzes the reaction

$$\text{Fru-6-P} + \text{ATP} \rightarrow \text{Fru-1,6-P}_2 + \text{ADP}$$

The reaction rate is assumed to depend on the concentrations of the two substrates, the product Fru-1,6-P_2 and the activator Fru-2,6-P_2. To cope with the regulatory complexity of the PFK-1 catalyzed reaction, we make the simplifying assumption that the overall rate ν_1 can be written as the product of three nonlinear factors:

$$\nu_1 = r_1 \cdot r_2 \cdot r_3$$

where r_1 accounts for the interaction of PFK-1 with ATP and Fru-2,6-P_2, r_2 accounts for the interaction of PFK-1 with Fru-6-P and Fru-2,6-P_2, and r_3 accounts for the interaction of PFK-1 with Fru-1,6-P_2.

The individual contributions of the respective concentrations to the reaction rate were derived empirically from experimental results for rat liver PFK-1.[24] The substrate inhibition by ATP and the relief of this inhibition by the activator Fru-2,6-P_2 is expressed by

$$r_1 = c_1[\text{ATP}]/(c_2 + d([\text{ATP}]^3/([\text{Fru-2,6-P}_2]^3 + 0.001)))$$

where brackets denote concentration, and the c_i and d are constants. Figure 1a shows plots of r_1 in the absence and in the presence of Fru-2,6-P_2 (compare Figure 4b of ref 24).

The sigmoidal dependence of the reaction rate on the concentration of Fru-6-P_2 and the change toward a hyperbolic dependence caused by allosteric activator Fru-2,6-P_2 is expressed by

$$r_2 = [\text{Fru-6-P}]/c_5(1 + [\text{Fru-6-P}]/c_5)^3/(L/(1 + c_6[\text{Fru-2,6-P}_2]) + (1 + [\text{Fru-6-P}]/c_5)^4)$$

where L is the allosteric constant in the Monod-Wyman-Changeux model. Figure 1b shows plots of r_2 in the absence and in the presence of Fru-2,6-P_2 (Compare Figure 4a of ref 24).

The experimental finding that PFK-1 is activated by low concentrations of the product Fru-1,6-P_2 and inhibited by higher concentrations of this product is expressed by

$$r_3 = [\text{Fru-1,6-P}_2]^4/(c_7 + [\text{Fru-1,6-P}_2]^6)$$

Here, for simplicity, no dependence on the concentration of Fru-2,6-P_2 is included. Figure 1c shows a plot of r_3 (compare Figure 5 of ref 24).

The activator Fru-2,6-P_2 is formed in the reaction

$$\text{Fru-6-P} + \text{ATP} \rightarrow \text{Fru-2,6-P}_2 + \text{ADP}$$

catalyzed by the enzyme phosphofructo-2-kinase/fructose-2,6-bisphosphatase (PFK-2). This dual activity enzyme is assumed to be permanently in the dephosphorylated kinase form. For the rate ν_2 of this reaction, we assume Michaelis Menten kinetics in ATP:

$$\nu_2 = c_3[\text{ATP}][\text{Fru-6-P}]/(c_4 + [\text{ATP}])$$

Finally, we include first-order decay of ATP and Fru-1,6-P_2 according to the equations $\nu_3 = c_8[\text{ATP}]$ and $\nu_4 = c_9[\text{Fru-1,6-P}_2]$, respectively.

The above assumptions yield the following set of coupled ordinary differential equations:

$$\text{d[ATP]/d}t = a([\text{ATP}]_0 - [\text{ATP}]) - \nu_1 - \nu_2 - \nu_3$$

$$\text{d[Fru-6-P]/d}t = a([\text{Fru-6-P}]_0 - [\text{Fru-6-P}]) - \nu_1 - \nu_2$$

$$\text{d[Fru-1,6-P}_2\text{]/d}t = a([\text{Fru-1,6-P}_2]_0 - [\text{Fru-1,6-P}_2]) + \nu_1 - \nu_4$$

$$\text{d[Fru-2,6-P}_2\text{]/d}t = a([\text{Fru-2,6-P}_2]_0 - [\text{Fru-2,6-P}_2]) + \nu_2 \quad (1)$$

Subscript zero denotes stock solution concentration, and a is the pumping rate constant.

Results

To understand the dynamics of the model, we first investigate the various contributions of substrate and product concentrations to the rate of the PFK-1 reaction, ν_1. If the rate of the PFK-1 reaction is taken to depend on ATP, Fru-6-P, and Fru-2,6-P_2 but not on Fru-1,6-P_2 (i.e., r_3 is taken to be constant), then the resulting dynamics is a simple quasi-harmonic oscillation (Figure 2a). Compared to the relaxation oscillation discussed in the next paragraph, the frequency of this oscillation is high and the amplitude small. If, starting at low values, the flow rate is increased, the oscillation is generated from the steady state in a supercritical Hopf bifurcation.

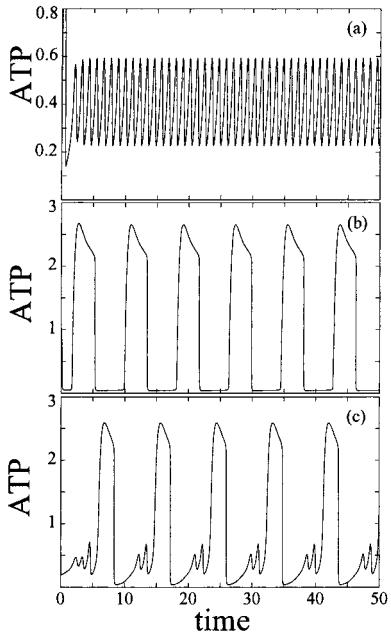

Figure 2. Time series in the model eq 1. (a) No dependence of rate ν_1 on [Fru-1,6-P_2] ($r_3 = 1$). (b) No dependence of rate ν_1 on [Fru-6-P] ($r_2 = 0.6$). (c) Full model. Parameters: $a = 0.82$, $[ATP]_0 = 10.6$, [Fru-6-P]$_0 = 10.4$, [Fru-1,6-P_2]$_0 = 1.15$, $c_1 = 29$, $c_2 = 0.1$, $c_3 = 1$, $c_4 = 0.1$, $c_5 = 1$, $c_6 = 19$, $c_7 = 0.1$, $c_8 = 1$, $c_9 = 10$, $d = 1$, $L = 80$.

The contribution of the ATP concentration in r_1 of eq 1 (i.e., for a fixed value of $r_2 \cdot r_3$) shows strong forward inhibition. This creates two coexisting stable steady states, one with low and one with high concentration of ATP, in accordance with the experimental results of ref 4. The forward inhibition is released in the presence of Fru-2,6-P_2 (Figure 1a). Taken together, these two features can already lead to oscillatory solutions of the components of the model. This oscillator produces relaxation oscillations of large amplitude and low frequency (as compared to the above-mentioned quasi-harmonic oscillations) for a wide range of parameters, e.g., the flow rate. During the oscillation Fru-2,6-P_2 causes the system to switch autonomously between the low and the high concentration level of ATP. The relaxation oscillation is preserved if the dependence of the rate ν_1 on the product Fru-1,6-P_2 is added, i.e., if only r_2 is taken to be constant. Figure 2b shows a time series of this extended subsystem. If the flow rate is used as a bifurcation parameter for this subsystem, it is found that the oscillatory domain is hemmed in by steady-state solutions. At the lower critical flow rate, the transition from a steady state to oscillations with finite amplitude is sharp with no coexistence of attractors. Close to this critical flow rate, the stable steady state is excitable; i.e., small perturbations suffice to induce one large amplitude spike of, e.g., ATP. At the higher critical flow rate, a parameter range with coexistence of steady state and oscillation is observed, but this region is not considered further in the present study.

Considering the full model eq 1, we find complex periodic oscillations as depicted in the time series Figure 2c. It can be seen that this complex oscillation is composed of small sinusoidal oscillations (as in Figure 2a) and large relaxational spikes (as in Figure 2b). In the example shown, a single large oscillation is followed by two small oscillations, and this behavior can be termed a 1^2 cycle.

Figure 3 displays two bifurcation diagrams of the full model eq 1. The maxima of the ATP oscillations are plotted as a function of the flow rate *a*. The bifurcation diagram for a feedstock concentration of Fru-1,6-P_2 = 1.155 (Figure 3a) reveals a large number of complex periodic and chaotic regimes

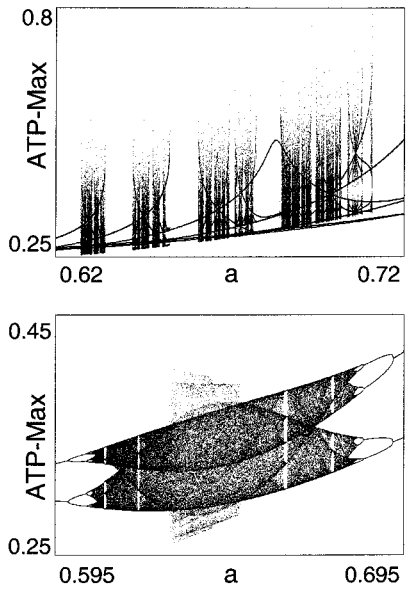

Figure 3. Bifurcation diagrams of eqs 1 as a function of flow rate *a*. (a) [Fru-1,6-P_2]$_0 = 1.155$, $c_1 = 33$. (b) [Fru-1,6-P_2]$_0 = 1.18$, $c_1 = 33$. Other parameters as in Figure 2.

in a close neighborhood to each other. At lower flow rates ($a < 0.62$), the system settles to a fixed point with high ATP concentration and low Fru-1,6-P_2 concentration. At higher flow rates ($a > 0.72$), there is a wide range of this parameter for which complex periodic oscillations occur before the system finally reaches simple periodic relaxation oscillations (similar to those in Figure 2b). Within the complex periodic region, part of the regimes are ordered in a period-adding sequence. For instance, starting at $a = 0.75$, we observe the sequence 1^3, 1^2, 1^1, 1^0 as *a* is increased. This bifurcation behavior is qualitatively maintained for a finite range of parameter [Fru-1,6-P_2]$_0$.

For a higher constant value of [Fru-1,6-P_2]$_0$, the qualitative behavior of the system can be seen in the bifurcation diagram Figure 3b. Here, the system undergoes a period-doubling sequence to chaos and a reverse period-doubling sequence back to simple periodic behavior with *a* as a bifurcation parameter. Within the chaotic region, there are windows of periodic behavior, and there are points of interior crisis where the amplitude of the chaotic oscillations changes abruptly (center of figure). In Figure 3b, for $a < 0.628$ and $a > 0.647$, the behavior is exclusively composed of small oscillations which are either periodic or chaotic. Between $a \approx 0.628$ and $a \approx 0.647$, the time series contains oscillations which are of larger amplitude but still considerably smaller than the above-mentioned relaxation oscillations. The system is in a steady state for low flow rates ($a < 0.59$) and has a broad region of complex periodic oscillations (composed of small sinusoidal and large relaxational peaks) at flow rates $a > 0.75$. This bifurcation behavior is qualitatively maintained for a finite range of parameter [Fru-1,6-P_2]$_0$.

Figure 4 shows two chaotic time series of the ATP concentration for parameters chosen from the bifurcation diagrams Figure 3. In Figure 4a, the small-amplitude chaos is of the ordinary type frequently encountered in low-dimensional chemical or biochemical systems. An attractor is characterized by a continued nonperiodic sequence of oscillations, close filling of planes in phase space by the trajectory, and occasional subharmonic deviations from an unstable period one cycle (see, e.g., the center of time series Figure 4a). The return map is a characteristic nearly one-dimensional curve with the first layers of a fractal set (not shown).

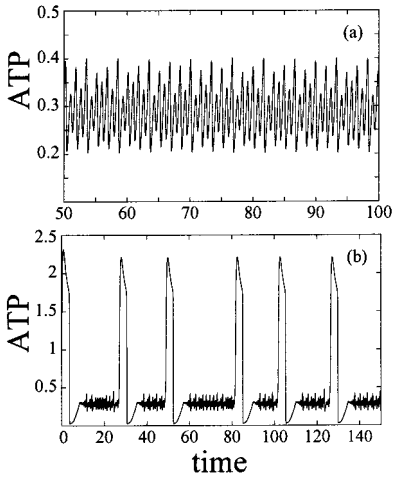

Figure 4. Chaotic time series of [ATP] with $a = 0.675$, and $c_1 = 33$. (a) [Fru-1,6-P_2]$_0 = 1.18$. (b) [Fru-1,6-P_2]$_0 = 1.155$. Other parameters as in Figure 2.

In Figure 4b, one sees that the small-amplitude, high-freqency chaos occurs on a low level of ATP mean concentration and that this chaos is interrupted irregularly by large ATP spikes. After a spike, the system returns to the small-amplitude chaos. During this small-amplitude chaos, the product [Fru-1,6-P_2] stays on a high level, while during the large-amplitude bursts of ATP, the concentration of Fru-1,6-P_2 decreases to a value near zero. The steep decrease in ATP is accompanied by a sharp spike of Fru-1,6-P_2. This chaotic attractor looks similar in the region of low ATP mean concentration but in addition contains large loops originating from the large-amplitude spikes. Both types of chaotic oscillations yield one positive Lyapunov characteristic exponent and a Lyapunov dimension between two and three.

An important feature of complex deterministic systems which distinguishes their behavior from random fluctuations is their response to external perturbations. Figure 5 shows responses of the model to two kinds of simulated perturbations. In Figure 5a, the autonomous system is in the small-amplitude chaotic state. At the point indicated by the arrows, a sudden small increase in ATP causes a perturbation. The response of the system is either hardly visible (first perturbation) or a large-amplitude relaxation oscillation after which the system returns to its original chaotic attractor (second perturbation). There is a threshold for the ATP perturbation to ignite this response, but its exact value depends on the phase of the chaotic oscillation at which ATP is added. This implies an escape region with complex topology in phase space from which the trajectory enters a spike. For stronger perturbations that cause the system to leave the region of small-amplitude chaos, it reliably responds with a large-amplitude spike in ATP. Similarly, an above-threshold addition of [Fru-1,6-P_2]$_0$ leads to a large-amplitude spike in ATP.

A different type of response to perturbations is observed when the autonomous system is in a steady state with a high level of ATP (Figure 5b). The value of the flow rate is located near the onset of oscillatory behavior. In both perturbation experiments, following an addition of ATP, the ATP concentration rapidly descends to a low value, starts to oscillate chaotically with small amplitude, and, after some time, spontaneously returns to the former steady state. However, due to the chaotic nature of the transient oscillations, the duration of the excursions varies strongly and unpredictably if the same perturbation is applied again. Similar observations are made if this steady state is perturbed by the addition of [Fru-1,6-P_2]$_0$.

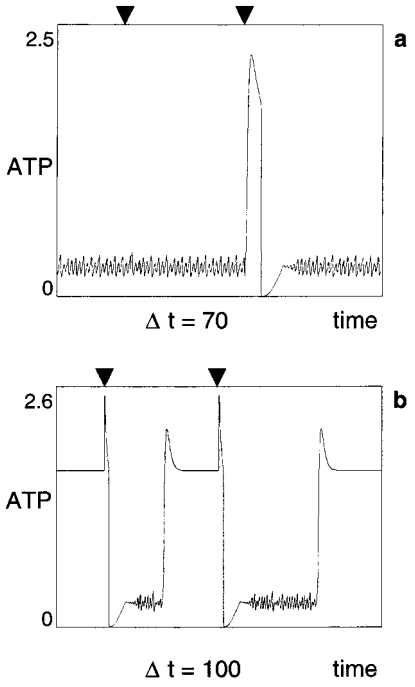

Figure 5. [ATP] time series with perturbations at the time indicated by arrows. (a) $a = 0.675$, [Fru-1,6-P_2]$_0 = 1.18$, $c_1 = 33$; perturbation of [ATP] to 0.4 for $\delta t = 0.1$. (b) $a = 0.65$, [Fru-1,6-P_2]$_0 = 1.15$, $c_1 = 29$; perturbation of [ATP] to 2.5 for $\delta t = 0.1$. Other parameters as in Figure 2.

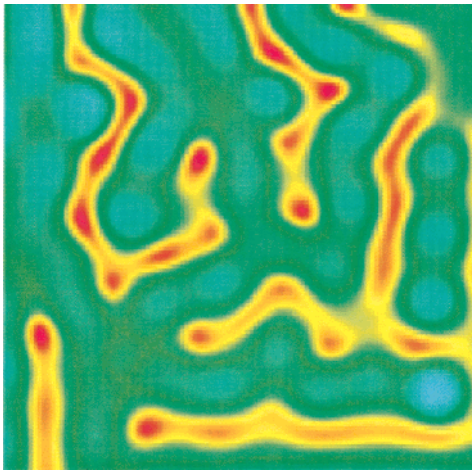

Figure 6. Snapshot of [ATP] distribution during small-amplitude labyrinth in the two-dimensional model (125×125 oscilators with next-neighbor coupling and zero-flux boundary conditions). $a = 0.675$, [Fru-1,6-P_2]$_0 = 1.20$, $c_1 = 33$, diffusion coefficients $D_{ATP} = 9.0$, $D_{Fru-6-P} = 14.0$, $D_{Fru-1,6-P_2} = D_{Fru-2,6-P_2} = 13.0$. Other parameters as in Figure 2. Color coding from dark blue ([ATP] = 0.2) to red ([ATP] = 0.45).

We extended the model of eq 1 into a system of diffusively coupled oscillators with two spatial dimensions. The diffusion coefficients were chosen such that Fru-6-P diffuses faster than both Fru-1,6-P_2 and Fru-2,6-P_2, and these in turn diffuse faster than ATP. So they reflect qualitatively the ratio of the molecular weights of the involved molecules. Using the kinetic parameters of Figure 2a,b, we found that for the set of diffusion coefficients given in Figure 6 the system establishes a spatially homogeneous oscillating concentration distribution from randomly chosen initial conditions; i.e., the system with parameters of Figure 2a showed periodic small-amplitude sinusoidal-like oscillations and with parameters of Figure 2b periodic large-amplitude relaxation

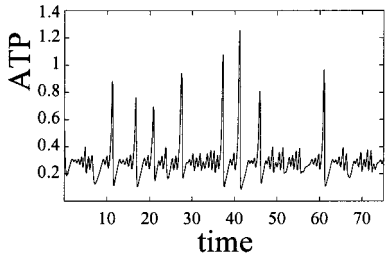

Figure 7. Time series of chaotic spiking of [ATP] of one oscillator in the spatially extended model. [Fru-1,6-P_2]$_0$ = 1.12, all other parameters as in Figure 6.

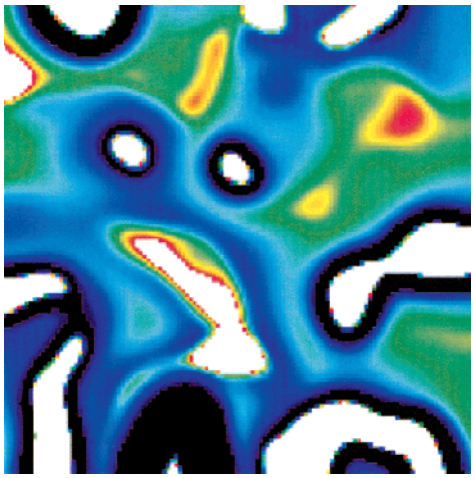

Figure 8. Snapshot of [ATP] distribution during chaotic spiking in the two-dimensional model. All parameters as in Figure 7. Color coding from dark blue ([ATP] = 0.2) to red ([ATP] = 0.45). White areas, [ATP] > 0.45; black areas, [ATP] < 0.2. Amplitudes in white areas reach values up to 2.3.

oscillations. Kinetic parameters as in Figure 2c lead to a homogeneous oscillation of type 1[3].

Choosing the kinetic parameters as in Figure 4 and varying [Fru-2,6-P_2]$_0$, spatially irregular concentration patterns were found in the extended system with zero-flux boundary conditions. Figure 6 shows the distribution of ATP at one instant during a regime in which an isolated oscillator displays chaotic small-amplitude oscillations. The spatial chaos for [Fru-2,6-P_2]$_0$=1.20 is a labyrinthine pattern with superimposed counter-oscillations of wave crests and troughs. Occasionally, transient activity occurs that is reminiscent of a broken multi-armed spiral (of equally small amplitude). This state is excitable like the small-amplitude chaos of Figure 5a. However, a local perturbation results exclusively in local spots of high ATP concentration. No traveling waves are induced by these spikes.

At a value [Fru-2,6-P_2]$_0$=1.12, a different type of chaotic spatio-temporal pattern is found. The behavior of a single oscillator in this case consists of a mixture of small- and large-amplitude oscillations (see Figure 7a). However, compared to Figure 4b, the amplitude and the shape of the large spikes in this case varies strongly. In space, we see remnants of the irregular labyrinthine waves of small amplitude and transient localized spots of large ATP amplitude (white areas in Figure 8). The amplitude inside these spots may reach values up to 2.2. These transient spots disrupt the small-amplitude waves irregularly. Decreasing [Fru-2,6-P_2]$_0$ further, the spots become wider, and they tend to maintain a high local concentration of ATP for a longer period. The spatial distribution of the variables reflects an important control property of the model. ATP concentration stays at a low level as long as Fru-2,6-P_2 is high because this releases the forward inhibition of ATP. ATP spots

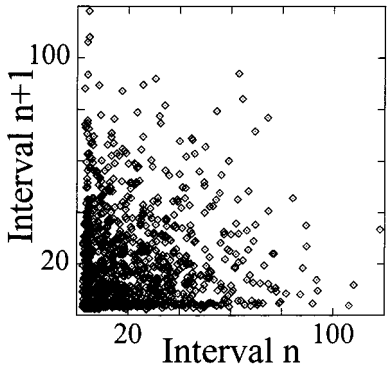

Figure 9. Return map of inter-spike-intervals for a single oscillator in the system of Figure 7. Only events with an amplitude larger than 0.7 were taken into account.

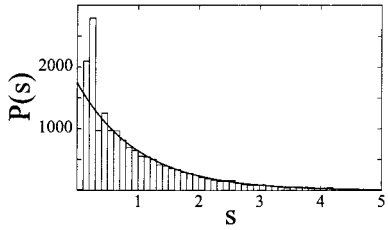

Figure 10. Nearest-neighbor spacing distribution $P(s)$ in a spatially extended system with periodic boundary conditions. Only spikes with an amplitude larger than 0.7 were considered. Spikings from time series of 25 oscillators distributed over the system were taken to improve the statistics. The dashed line is the theoretically obtained Poisson distribution.

grow only when the concentration of Fru-2,6-P_2 is diminished, thus enhancing the forward inhibition and in effect causing ATP accumulation. Each spot is surrounded by a trough of low ATP concentration (black ribbon around white spot in Figure 8) that prevents it from spreading into the surrounding medium. Taking parameters as in Figure 8 and increasing the diffusion coefficient of Fru-6-P to $D_{\mathrm{Fru-6-P}}$ = 25.0, a stable Turing pattern of irregularly distributed spots is observed.

It has to be added that for [Fru-2,6-P_2]$_0$ = 1.12 this self-exciting chaotic behavior is not the only stable solution of the system. For certain choices of initial conditions, an oscillating labyrinthine patterns develops that appears to settle to a period-2 oscillation. In this case, the system is spatially inhomogeneous, but no spiking with large amplitude is observed for the time of integration.

Figure 9 is a return map obtained from inter-spike-intervals (ISIs) of the chaotically spiking state in Figures 7 and 8. The result for a single site is a diffuse distribution of ISIs with no discernible structure that would indicate the presence of low-dimensional chaos. Note, however, that in this case all maxima that are due to quasi-harmonic small-amplitude "background oscillations" were deliberately omitted (as is the custom in the analysis of neural firing). Figure 10 presents the distribution $P(s)$ of the probabilities to find two consecutive events at a temporal interval s, where s is given in units of the mean distance between two spikes on the unfolded time scale (see ref 25 for a recent introduction to this type of analysis). The values of $P(s)$ were normalized to the total number of spikes (about 18000). The distribution is characterized by a gap for very short intervals due to the presence of a refractory period after each spike. This in return causes an overshoot at an interval of about 0.2. At intervals larger that 0.6, the distribution almost perfectly follows the theoretical curve for a Poisson distribution, i.e., a truely random process.

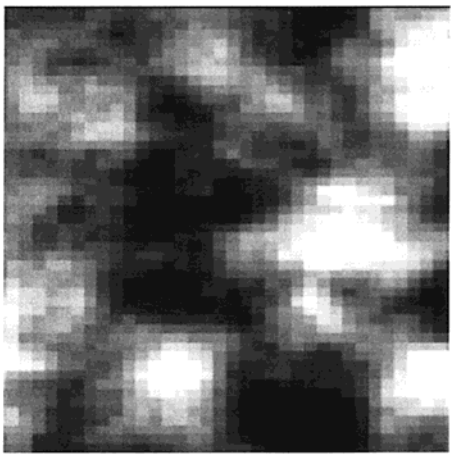

Figure 11. Distribution of the times each oscillator spend with [ATP] > 0.7. Simulation of a 50 × 50 net with periodic boundary conditions to avoid boundary artifacts during a period of 2500 units of model time. Grading coding from white (41.8 time units) to black (78.3 time units).

A remarkable feature of the spots in the chaotic spatiotemporal chaos of Figures 7 and 8 is that, even though they do not occur at a fixed position in the long run, they have a strong tendency to reappear at the same or a rather nearby location for some time. A consequence of this is that depending on the time scale chosen, a time series can either show a large (black) or a small (white) average frequency of spiking. Figure 11 is a map of the average time of each oscillator spent at a concentration of ATP higher than 0.7. The map was obtained in the time window $22.5 \times 10^3 < t < 25 \times 10^3$, ensuring that no transient effects are recorded. The maximal average time is about twice the minimal average time spent with high levels of ATP. A distribution recorded for the same interval of time is distinctly nonuniform, independent of when the sampling is started. The location of the different areas changes as a function of the time window chosen. The system thus not only spontaneously develops but also maintains for considerable times areas with strongly increased ATP concentration.

The distribution of black and white areas as in Figure 11 is a function of the chosen initial conditions. However, due to the excitable nature of the system during the low-amplitude labyrinthine waves, local inhomogeneities can be exploited to generate preferred areas of (for instance) high average ATP concentration. An area where the local influx of ATP is increased (increased value of $[ATP]_0$) will predictably become black due to its increased frequency of spiking.

Discussion

The model eq 1 describes a set of biochemical reactions which include qualitative features of the reactions catalyzed by PFK-1. In the absence of Fru-2,6-P_2, this model reproduces the experimentally observed bistability (i.e., two coexisting stable steady states[4]) due to forward inhibition of the activity of PFK-1 by ATP and the autocatalytic acceleration by product Fru-1,6-P_2. On one hand, the Fru-1,6-P_2 backward activation leads to an oscillation with small amplitude by means of a Hopf instability of the low ATP steady state (Figure 2a). On the other hand, the regulation of the ATP forward inhibition by Fru-2,6-P_2 results in a periodic oscillation with large amplitude (Figure 2b). This latter oscillation can be understood as an autonomous switching of the system between the two formerly stable steady states.

Taken together, these three features (bistability, Hopf instability of one of the states, and autonomous switching between small oscillation and upper steady state) provide the dynamic mechanism by which Fru-2,6-P_2 regulation of the PFK-1 reaction generates complex oscillations. Simulations with different sets of parameters and with modified model equations indicate that this mechanism is a generic feature of enzymatic reaction systems with regulatory properties as in Figure 1. In particular, whereas simple oscillations can also be found in the absence of Fru-2,6-P_2, joining of the two distinct types of oscillations to yield excitable chaos and self-excitation is only accomplished by the regulation of Fru-2,6-P_2.

During complex periodic oscillations in the homogeneous system, the concentration of ATP either oscillates with small amplitude at a low level or undergoes a relaxation at a level which is approximately 10 times higher. The interval between two large spikes depends on the number of small amplitude oscillations. This allows a stepwise tuning of this interval as a function of control parameter. For example, in the region with period-adding behavior, the interval can be increased as flow parameter a is decreased. In the parameter region of Figure 3a, other possibilities exist. The complex periodic behavior can be of the form 1^m1^n, where m and n are the numbers of small oscillations between two large spikes. Thus, a complete period consists of one spike, m small oscillations and a second spike followed by n small oscillations. In the chaotic regions, these periods are irregularly distributed. It should be noted, however, that even in this chaotic case the maxima of [ATP] are almost the same and their tiny variation would not be detectable under experimental conditions with intrinsic noise. The concentration of ATP would thus produce an irregular spike train reminiscent of nerve cell behavior.

The model reproduces the experimental observation (in yeast extracts) that the amplitude of small oscillations increases between large peaks (as in Figure 2c), and also, there are indications of regimes with chaotic small oscillations between large peaks (as in Figure 4b) in the recordings of ref 15. With the present set of parameters, we have not seen the combination of multiple large peaks and small peaks (as, e.g., 3^2). However, such sequences are likely to occur in some neighborhood of the parameter space if the slow-manifold structure depicted in ref 26 applies.

Chaotic oscillations in a homogeneous glycolytic model were reported in ref 27. This model shows a transition from toroidal oscillations to chaos on a distorted two-torus when two time-delays are introduced. So far, toroidal oscillations have not been reported in glycolytic systems. The experimental toroidal behavior referred to in ref 27 was the result of periodic forcing of a limit cycle and was not found in the autonomous system. Our simulations indicate that the complex oscillations reported here are not the result of a smooth or fractalized torus in phase space but are located on a folded slow manifold as discussed in ref 26. However, this does not exclude the possibility of toroidal solutions in our model at other sets of parameters.

The complex patterns observed experimentally in yeast cell extracts point to the presence of corresponding attractors which therefore have to be explained by models. Under nonstationary conditions, transient complex periodic and chaotic oscillations were found in the cerium-catalyzed Belousov−Zhabotinsky reaction,[28] where the presence of complex periodic and chaotic attractors under stationary conditions was well-established. Our bifurcation diagram in the region of small amplitude oscillations (Figure 3b) shows a period-doubling sequence into chaos and the reverse sequence out of chaos. Thus, if parameter a is driven slowly through this region, the resulting time series shows an corresponding sequence of oscillations from periodic to chaotic

and back to periodic. Sequences in to and out of chaos with indications of period-doublings are thus to be expected under shifting (nonstationary) experimental conditions; e.g. it is conceivable that in an experiment some reaction rate changes slowly during the course of the time (for instance, caused by a slow change of an enzymatic activity) and thus acts as an intrinsic bifurcation parameter. In an in vivo environment, it is even more likely that some conditions will change with time and transient dynamic behavior might be the rule rather than an exception in living organisms. Only in well-controlled in vitro experiments in an open reactor is it possible to maintain complex periodic and chaotic behavior for a relatively long time (for a nonglycolytic example, see ref 29). Furthermore, it is known that the mere presence of spatial degrees of freedom can increase a system's dynamics considerably.[8]

It can therefore not be expected that a long stationary time series such as Figure 4 can easily be obtained from an in vivo recording. Traditional methods of time series analysis like phase diagrams, return maps, and calculations of Lyapunov exponents and dimensions will then not be applicable with good reliability. At least two things can be done, however, to test whether experimentally observed complex variations of some metabolite are caused by deterministic nonlinear dynamics or by nondeterministic fluctuations. First, complex periodic oscillations are generically surrounded by simple periodic regimes in parameter space. It is very likely then that both types of behavior will be found under similar experimental conditions and their qualitative differences can be compared to model calculations. Second, complex deterministic systems show unique responses to external perturbations. In the present model, in an oscillatory regime without large oscillations, a large-amplitude spike can be induced as in an excitable system (Figure 5a). In the case of a stable steady-state complex, oscillatory responses can be obtained when the oscillatory domain is nearby in parameter space (Figure 5b). In both tests, the noise level can be assumed to stay constant.

The spatio-temporal extension of the model generates an overwhelming number of spatio-temporal patterns, both periodic and chaotic. In the present contribution, we have constrained ourselves to a subset of complex patterns with surprising properties that might have implications for the role of ATP in metabolic information processing. First, a state of excitable spatio-temporal chaos was found (Figure 6). This regime creates ongoing fluctuations of the basal state from which characteristic spikes can be elicited. Excitable spatio-temporal chaos also occurs in spatially extended models of cytosolic calcium oscillations.[30] However, in the case of calcium ion concentration, continued excitation of the basal chaos induces periodic traveling waves that propagate through the whole system. In contrast, the ATP spots accompanying the spikes occur locally and prohibit any spreading of waves. This is achieved by a center-surround mechanism with activation of a central core and lateral inhibition in a neighborhood surrounding the core (see, e.g., ref 31 for an experimental observation of center-surround characteristics in the activity of the visual receptive field in frogs). In our case, this can be understood by the interaction of ATP with the regulator F-2,6-P_2. In the center, a low concentration of F-2,6-P_2 allows accumulation of ATP caused by its forward inhibition. The surrounding environment, on the other hand, has a high concentration of F-2,6-P_2 that releases the forward inhibition and thus diminishes the concentration of ATP to a level below that of the small-amplitude oscillations. Consequently, in this region, the system shows strongly reduced excitability. If a source of ATP would increase its production locally (for instance a mitochondrion), the result would be continued spiking and therefore a region of far-above-average concentration of ATP. Thus, near the threshold of the excitable chaos, inhomogeneities would lead to strong local amplification of ATP. Likewise, a locally diminished influx of F-2,6-P_2 can cause spots of far-above-average concentrations. Both supplies therefore can be considered dynamic on−off switches for ATP.

Second, at lower values of $[\text{F-2,6-P}_2]_0$ the spatio-temporal system can be self-exciting (Figure 8). In this case, the spikes and spots occur spontaneously. From a dynamical point of view, the nearby existence of periodic as well as Turing patterns suggests that this regime owes its existence to a Hopf-Turing mixed mode regime (cf. ref 32). As is discussed in more detail in ref 30, this kind of spatio-temporal (hyper-)chaos generically occurs in extended biochemical systems. In the present system, the combination of an irregular oscillatory basal state with the transient aparition of an irregular Turing pattern is exploited to induce aperiodic self-excitation. This chaotically spiking regime neither permits target waves nor spiral waves to propagate in space as would be expected for an ordinary excitable medium. Thus, following the results on propagating calcium waves,[30] a second type of spatio-temporal excitable chaos has been found. This second type behaves essentially like a random spike-and-spot generator when only the large-amplitude spikes are considered. Neither ISI maps (Figure 9) nor ISI distribitions (Figure 10) provide any clues to the deterministic origin of this behavior. However, as was pointed out in ref 33 for the homogeneous case of excitable chaos, this self-exciting chaos would respond differently to the presence of random perturbations. In that case, the increased spiking frequency would be accompanied by an increase of order in the return map as well as the appearance of correlations in the next-neighbor distribution $P(s)$.[33]

The mean distribution of the concentration of ATP in the absence of any inhomogeneity or perturbation remains inhomogeneous for long (but less than infinite) times even though one could expect a homogeneous mixing of the chaotic flow for time approaching infinity. This inhomogeneous mean distribution (Figure 11) implies a "memory effect": once a spot is initiated (e.g., by the choice of random initial conditions) there is an increased probablity of observing another spot at or near the center of the first spot. In contrast, areas between "first spots" are less likely to generate a spot. In the very long run, this imbalance is washed out because the dark regions of Figure 11 are not static but glide into the white regions albeit at very low velocity. In the more realistic situation of a nonhomogeneous field (e.g., due to the distribution of ATP-producing mitochondria in a living cell), this could easily translate into a stable irregular distribution of spots of increased concentration of ATP.

Rather than being mere artifacts of nonlinear kinetics, glycolytic oscillations are likely to serve a function in vivo. For instance, in ref 34, it was suggested that glycolytic oscillations may cause oscillations in cytosolic calcium ions and insulin release in pancreatic islets. Recordings of oscillatory lactate in β-cells seem to indicate oscillatory glycolytic dynamics.[35] Possibly confirming this hypothesis, oscillations of the ATP/ADP ratio and of Fru-6-P were reported in a β-cell suspension.[36] In recent experiments on spatio-temporal oscillations of NADH and pH in neutrophils (bacteria-ingesting white blood cells), it was hinted at a possible glycolytic origin and it was speculated that they could be accompanied by patterns of ATP concentration in the service of cellular information processing.[37,38] In this sense, well-defined patterns of ATP spots

and spiking sequences could serve as dynamic stimulation for other ATP-dependent metabolic processes. New experimental techniques that would allow the continuous recording of adenosine phosphates with high spatial resolution (e.g., exploiting the vibrational differences of the phosphate groups in the IR) are required to confirm or reject this hypothesis.

Finally, the range of complexity of spatio-temporal glycolytic patterns (from period one to "random") in our model suggests that concentration patterns of different complexities would be available to carry qualitatively different pieces of information (as was proposed for the experimentally observed periodic and chaotic calcium oscillations in rat hepatocytes[13]). The regulatory properties of Fru-2,6-P_2 could then serve as metabolic means to switch between various dynamic regimes and glycolysis would actively function to provide the crucial kinetic backbone for the metabolic pattern formation.

Acknowledgment. We thank Hans Degn, Lars Olsen, Ursula Kummer, Sune Danø, and Thomas Mair for fruitful discussions. G.B. gratefully acknowledges financial support from the Danish Research Society during a stay at Odense University and from CONACyT, Mexico (catedra patrimonial II). M.M. gratefully acknowledges financial support from CONACyT, Mexico (Project 32101-E).

References and Notes

(1) Chance, B.; Hess, B.; Betz, A. *Biochem. Biophys. Res. Commun.* **1964**, *16*, 182.
(2) Frenkel, R. *Arch. Biochem. Biophys.* **1968**, *125*, 166.
(3) Tornheim, K.; Lowenstein, J. M. *J. Biol. Chem.* **1973**, *248*, 2670.
(4) Frenzel, J.; Schellenberger, W.; Eschrich, K. *Biol. Chem. Hoppe-Seyler* **1995**, *376*, 17.
(5) Rössler, O. E. *Z. Naturforsch. A* **1976**, *31*, 1168.
(6) Baier, G.; Sahle, S.; Kummer, U.; Brock, R. *Z. Naturforsch. A* **1994**, *49*, 835.
(7) Strasser, P.; Rössler, O. E.; Baier, G. *J. Chem. Phys.* **1996**, *104*, 9974.
(8) Baier, G.; Sahle, S. *J. Theor. Biol.* **1998**, *193*, 233.
(9) Lechleiter, J.; Girard, S.; Peralta, E.; Clapham, D. *Science* **1991**, *252*, 123.
(10) Mair, T.; Müller, S. C. *J. Biol. Chem.* **1996**, *271*, 627.
(11) Mair, T.; Warnke, C.; Müller, S. C. *Faraday Discuss.*, in press.
(12) Green, A. K.; Cobbold, P. H.; Dixon, J. K. *Biochem. J.* **1995**, *310*, 629.
(13) Kummer, U.; Olsen, L. F.; Dixon, C. J.; Green, A. K.; Bornberg-Bauer, E.; Baier, G. *Biophys. J.* **2000**, *79*, 1188.
(14) Nielsen, K.; Sørensen, P. G.; Hynne, F. *J. Theor. Biol.* **1997**, *186*, 303.
(15) Nielsen, K.; Sørensen, P. G.; Hynne, F.; Busse, H.-G. *Biophys. Chem.* **1998**, *72*, 49.
(16) Van Schaftingen, E.; Hue, L.; Hers, H. G. *Biochem. J.* **1980**, *192*, 887.
(17) Decroly, O.; Goldbeter, A. *Proc. Natl. Acad. Sci. U.S.A.* **1982**, *79*, 6917.
(18) Markus, M.; Hess, B. *Proc. Natl. Acad. Sci. U.S.A.* **1984**, *81*, 4394.
(19) Smolen, P. *J. Theor. Biol.* **1995**, *174*, 137.
(20) Yuan, Z.; Medina, M. A.; Boiteux, A.; Müller, S. C.; Hess, B. *Eur. J. Biochem.* **1990**, *192*, 791.
(21) Tornheim, K. *J. Biol. Chem.* **1988**, *263*, 2619.
(22) Schellenberger, W.; Eschrich, K.; Hofmann, E. *Biochem. Biophys. Res. Commun.* **1985**, *126*, 571.
(23) Frenzel, J.; Schellenberger, W.; Eschrich, K. *FEBS Lett.* **1996**, *390*, 229.
(24) Hers, H. G.; Van Schaftingen, E. *Biochem. J.* **1982**, *206*, 1.
(25) Flores, J.; Horoi, M.; Müller, M.; Seligman, T. H. *Phys. Rev. E* **2000**, *63*, 026204.
(26) Goryachev, A.; Strizhak, P.; Kapral, R. *J. Chem. Phys.* **1997**, *107*, 2881.
(27) Martinez de la Fuente, I.; Martinez, L.; Veguillas, J.; Aguirregabiria, J. M. *Biophys. J.* **1996**, *71*, 2375.
(28) Wang, J.; Sørensen, P. G.; Hynne, F. *J. Phys. Chem.* **1994**, *98*, 725.
(29) Kummer, U.; Hauser, M.; Wegmann, K.; Olsen, L. F.; Baier, G. *J. Am. Chem. Soc.* **1998**, *119*, 22084.
(30) Baier, G.; Sahle, S.; Chen, J.-P.; Hoff, A. A. *J. Chem. Phys.* **1999**, *110*, 3251.
(31) Barlow, H. B. *J. Physiol. (London)* **1953**, *119*, 58 and 69.
(32) De Wit, A.; Dewel, G.; Borckmans, P. *Phys. Rev. E* **1993**, *48*, R4191.
(33) Baier, G.; Escalera Santos, G. J.; Perales, H.; Rivera, M.; Müller, M.; Leder, R.; Parmananda, P. *Phys. Rev. E* **2000**, *62*, 7579.
(34) Longo, E. A.; Tornheim, K.; Deeney, J. T.; Varnum, B. A.; Tillotson, D.; Prentki, M.; Corkey, B. E. *J. Biol. Chem.* **1991**, *266*, 9314.
(35) Chou, H. F.; Berman, N.; Ipp, E. *Am. J. Physiol.* **1992**, *262*, E800.
(36) Nilsson, T.; Schultz, V.; Berggren, P.-O.; Corkey, B. E.; Tornheim, K. *Biochem. J.* **1996**, *314*, 91.
(37) Petty, H. R.; Worth, R. G.; Kindzelskii, A. L. *Phys. Rev. Lett.* **2000**, *84*, 2754.
(38) Petty, H. R.; Kindzelskii, A. L. *Proc. Natl. Acad. Sci. U.S.A.* **2001**, *98*, 3145.